Supplementary Materials for

"Termite mounds can increase the robustness of dryland ecosystems to climatic change"

Juan A. Bonachela, Robert M. Pringle, Efrat Sheffer, Tyler C. Coverdale,
Jennifer A. Guyton, Kelly K. Caylor, Simon A. Levin & Corina E. Tarnita

correspondence to: ctarnita@princeton.edu

This PDF file includes:

Supplementary Text
Figs. S1 to S8
Table S1
Captions for Movies S1 to S2

Other Suplementary Materials for this manuscript includes the following:

Movies S1 to S2

Supplementary Text

1 Theoretical component

Here we scrutinize different aspects of the interaction between termite mounds, vegetation, and water in semi-arid ecosystems. More specifically, we aim to understand how the presence of termite mounds (a) alters vegetation spatial distribution and shape, and (b) affects the robustness (or resilience, see text) of the ecosystem under changing environmental conditions, potentially modifying the susceptibility and behavior of the ecosystem close to the desertification point (that is, close to a so-called "catastrophic shift").

To this end, we choose a theoretical reaction-diffusion model widely used to study vegetation patterns in semi-arid ecosystems on homogeneous backgrounds, and modify it to account for the heterogeneity introduced by the presence of termites in terms of nutrients and water dynamics on versus off mounds. Finally, we compare the performance of both the original and the modified models under various (static and dynamic) environmental scenarios.

1.1 The base model

In this model taken from (10), three different interaction agents are present, namely plant biomass concentration, P (g m^{-2}), soil water concentration, W (mm), and surface water concentration O (mm). The interaction between these densities is given by:

$$\frac{\partial P(x,t)}{\partial t} = c\, g_{max} \frac{W}{W + k_1} P - d\, P + D_P \nabla^2 P \tag{1}$$

$$\frac{\partial W(x,t)}{\partial t} = \alpha \frac{P + k_2 W_0}{P + k_2} O - g_{max} \frac{W}{W + k_1} P - r_W W + D_W \nabla^2 W \tag{2}$$

$$\frac{\partial O(x,t)}{\partial t} = R - \alpha \frac{P + k_2 W_0}{P + k_2} O + D_O \nabla^2 O \tag{3}$$

In Eq. (1), the first term represents plant vegetation growth by means of water uptake (W is the only plant resource considered here); the second term, plant mortality; and the third term, diffusion as a result of, e.g. seed dispersal. Here, c is the conversion of water

uptake by plants to plant growth, g_{max} is the plant maximum uptake rate, k_1 represents a half-saturation constant of specific plant growth and water uptake, d is the specific loss of plant density due to mortality, and D_P the diffusivity constant giving plant dispersal (see units in table S1). In Eq. (2), the first term models the infiltration of surface water (and, therefore, its conversion into soil water); the second and third terms encode water uptake by plants and evaporation; and the last term represents water circulation into the ground. Here, α is the maximum rate of infiltration, k_2 represents the saturation constant of water infiltration, W_0 is part of the infiltration capacity of the soil in the absence of plants, r_W is the specific soil water loss due to evaporation and drainage, and D_W is the underground water diffusivity. The first term in Eq. (3) represents the accumulation of surface water coming from precipitation, the second term represents water infiltration into the ground, and the last term represents circulation on the surface. Here, R is the precipitation rate, and D_O is surface water diffusivity.

With the model above, varying the precipitation rate R produces the three main patterns observed in semi-arid ecosystems (under the assumption of homogeneous soils). For the parametrization in table 1, using the homogeneous plant-less solution as initial state, any initial perturbation will relax back to the homogeneous plant-less state if $R \leq 0.55(5)$ (number in parenthesis indicates confidence interval; e.g., in this case 0.55 +/– 0.05); however, for $R > 0.55(5)$, a sufficiently high perturbation containing all possible spatial frequencies (here we used one that perturbs randomly-selected locations in the system (10)) eventually produces a heterogeneous final state, with clumps (or spots) of vegetation for $R \in (0.55(5), 1.00(5))$; vegetation labyrinths if $R \in [1.00(5), 1.15(5))$; and bare-soil gaps for $R \in [1.15(5), 1.25(5))$ (Fig. S3 upper panel). Finally, a plant-full homogeneous state is reached for $R \geq 1.25(5)$.

The diffusion parameters are tuned, together with the integration space mesh dx, to scale the patterns as desired. For our simulations, we have used the values in the table for the diffusivities, with a corresponding $dx = 2$, $dx = 2 \times 10^{-1}$, $dx = 6 \times 10^{-2}$, and $dx = 2 \times 10^{-2}$ (in meters), respectively. For the most realistic parametrization, $dx = 10^{-2}$ m, together with the smallest values for the diffusivity parameters in table S1. We have tried a regular forward Euler integration scheme, and a more reliable, two-step Euler scheme; when the integration time mesh dt is sufficiently small, both yielded identical results.

1.2 Termite-mound-induced heterogeneity

We modify the previous model by introducing soil heterogeneity created by termite mounds. Termites affect their environment in two fundamental ways: (i) on and near mounds (henceforth referred to as ‘on-mounds’ for simplicity), termites accumulate nutrients, making them available for plants; (ii) similarly, due to their tunneling and transport of water as well as due to their modification of soil texture, termites increase soil moisture on-mounds. We refer to all regions away from any termite mounds as ‘off-mounds’. We incorporate this heterogeneity as follows:

i. Because water is the only resource in the reference model, the effects of an increase of nutrients are reflected implicitly via its effects on plant growth. We assume that plant growth is mediated by the interaction between water uptake and nutrients (i.e. the more nutrients, the more efficiently the same amount of water is converted into plant biomass); since c is the only parameter of the model that reflects the conversion of water uptake by plants into plant growth, we assume that differential nutrient availability is reflected in differential conversion factors. We will refer to c as "water-use efficiency". Here we consider two different models exploring the extremes of termite behavior.

Model 1: termites only have a positive effect on water-use efficiency, in the sense that they improve it on mounds but do not affect it off mounds; this corresponds to an idealized case. In this case, if c is the conversion factor in (10) and we let c_{off} be the conversion factor off mounds (independent of spatial location) and $c_{on}(x)$ be the conversion factor on mounds (dependent on distance x from the center of the termite mound):

$$c_{off} = c \qquad c_{on}(x) = cG(x) \tag{4}$$

where x is the distance to the mound center and G(x) gives the improvement as a function of the distance from the center of the mound; mathematically we express it as:

$$G(x) = \begin{cases} G_c & \text{for} \quad x \le r/2 \\ 1 + 2(G_c - 1)(1 - x/r) & \text{for} \quad r/2 < x \le r \\ 1 & \text{for} \quad x > r, \end{cases} \tag{5}$$

where r is the radius (measured from the center of the mound) on which the mound has an effect compared to off the mound, and G_c is the on-mound improvement factor. This introduces the space dependence of c as a flat enhancement on a radius of *r*/2 from the center of the mound, which then quickly decreases to baseline values at distances to the center between *r*/2 and r. It is simplified but consistent with the literature. The profile type for r = 5m is given by the red curve in the left panel of Fig. S1. We also explored a Gaussian function that peaks at the mound center and reaches zero at distances close to r from the center (green curve in the left panel of Fig. S1). We find that, qualitatively, the two functions give similar results; since the flat enhancement is likely to give a

more realistic description of the system, we will henceforth use it in our simulations.

Model 2: termites have a zero-sum effect, in the sense that any improvement in water-use efficiency on-mounds comes at the expense of a decrease off-mounds; this corresponds to a case where the nutrients accumulated on the mounds are taken from elsewhere off the mounds. In this case, using the same notation as above and in addition letting A_{off} be the total off-mound surface area, A_{on} be the total on-mound surface area and A be the total surface area (i.e. $A = A_{off} + A_{on}$), we require that:

$$cA = c_{off} A_{off} + \int_{A_{on}} c_{on}(x)\, dA_{on} \qquad \text{and} \qquad c_{on}(x) = cG(x) \tag{6}$$

where again G(x) gives the improvement as a function of the distance from the center of the mound, as in Eq. (5).

The latter model is the more conservative one and this is why in the main text we only present the results for it. However we expect the real effect of termites on their environment to be somewhere in between Model 1 and Model 2, which is why we study both here.

ii. To incorporate the effects on soil moisture, we have three options, all of which reflect the water dynamics: modify α or W_0 to reflect changes in how quickly water infiltrates into the soil, or modify k_2 to reflect the combined effect of bioturbation and plant density on water infiltration. For simplicity we will refer to k_2 as the 'infiltration effect'. All three yield qualitatively similar dynamics in our simulations, and therefore for simplicity we only modify k_2. Because k_2 acts as a half-saturation constant in the infiltration term, one achieves higher infiltration for a given plant density by decreasing k_2. Therefore, when we refer to k_2 as indicative of the infiltration effect, we implicitly mean that k_2 is negatively correlated with infiltration; moreover, when we refer to improvement for k_2, we mean that k_2 is decreased. Thus, to reflect the effect of termite mounds we let

$$k_{2,off} = k_2 \qquad k_{2,on}(x) = \frac{k_2}{G(x)} \tag{7}$$

where, similar to Eq. (5), G(x) provides the improvement as a function of the distance from the center of the mound, given by:

$$G(x) = \begin{cases} G_{k_2} & \text{for} \quad x \le r/2 \\ 1 + 2(G_{k_2} - 1)(1 - x/r) & \text{for} \quad r/2 < x \le r \\ 1 & \text{for} \quad x > r, \end{cases} \tag{8}$$

This is qualitatively identical to Eq. (5), but now modulated by G_{k2}, the k_2-related on-mound improvement factor. The larger G_{k2}, the larger the reduction in k_2 and, therefore, the improvement for the overall infiltration (for example, $G_{k2} = 1.5$ leads to a 67% reduction in k_2, that is, a 33% improvement).

Mounds at our field site, Mpala Research Centre (MRC), described in detail in Section 2, are separated by an average distance of about 50m (measured between centers of mounds) and they are overdispersed as a result of intraspecific competition. We have tried two spatial distributions for the mounds: a periodic one, in which mounds are located on a lattice of regularly spaced mounds with mesh 50m, and a more realistic configuration in which each mound has six neighbors placed in a configuration that resembles that of a hexagon (see right panel Fig. S1).

Both Model 1 and Model 2 as well as both pattern implementations above show a similar result: the emergent vegetation pattern is composed of a background pattern of the off-mound vegetation, that is mostly independent of the mound-induced heterogeneity), interrupted by more homogenous vegetation cover on the mounds; because the mounds are spatially patterned, the (homogeneous) vegetation associated with them is also spatially patterned at the larger scale of the mounds. In their immediate vicinity, mounds affect the vegetation that constitutes the transition between two patterns – there is a halo of almost barren ground (a diffusive boundary layer) resulting from the highly vegetated mound acting as a sink for nearby water (see Fig. S3 and Fig. 2C-E in the main text for the patterns). Fig. S2 shows the effects of the mounds on surface and soil water on- and off-mounds and Fig. 2B in the main text shows the same effects on vegetation biomass.

1.3 Study of ecosystem robustness

It is important to study the response of the whole ecosystem to different precipitation levels, in the presence and in the absence of termite mounds. This study will allow us to determine whether and how the presence of mounds affects the ecosystem. To this end, we sweep a wide range of constant precipitation levels, R, using as initial condition a natural state generated by the system itself, i.e. the final (stationary) state reached with the previous value of R. This allows us to discern two directions and separate an "increasing R" from a "decreasing R" case. In a system with a smooth transition from plant-less (desert, P = 0) final states to vegetated ($P \neq 0$) final states, the two directions

should yield an identical P vs R (phase) diagram. In a system with an abrupt transition (also called catastrophic shift), the two directions are different: falling into the P = 0 phase (desert) requires smaller R values than escaping from that phase, thus indicating that the same rainfall value R may provide a different result depending on the initial conditions (hysteresis and bistability).

Without mounds, the transition between phases is abrupt and the hysteresis cycle is evident, with the threshold for the increasing-R direction being much larger than the one for the decreasing-R (see Fig. S4 (A) and also Fig. 4 in the main text). On the other hand, with termite mounds present, for both Model 1 and Model 2, for the improvements of interest in this paper ($G_c = G_{k2} = 1.5$), we observe two hysteresis cycles (see Fig. S4 (B,C)): one corresponds to the loss/recovery of vegetation off mounds and is situated roughly between the same precipitation levels as in the no-mounds case, whereas the other – of much smaller area – corresponds to the loss/recovery of vegetation on mounds, and is situated at much lower precipitation levels. The main transitions from plant-less (desert) to plant-full (full vegetation cover) states showcasing the two hysteresis jumps, as well as their associated patterns, are shown in Fig. S3.

When termite mounds are present, the desertification thresholds are shifted to remarkably smaller values, for both Model 1 and Model 2. Moreover, there is some small but significant improvement in overall biomass production (~11% and ~7%, respectively, for the two models and parametrization shown in Fig. S4 (B,C), but hard to observe due to our use of a logarithmic y-axis). As expected, Model 2 is slightly less of an improvement than Model 1, but both perform significantly better than the no-mound case. Thus, the presence of termite mounds allows the vegetation in the ecosystem to perform and resist better in the face of rainfall scarcity when precipitation decreases (increased resistance of the ecosystem), and requires smaller precipitation rates to escape desert states (increased recovery of the ecosystem). In summary, the system becomes more robust (sensu (13): higher resistance and recovery) to total desertification, with mounds acting as reservoirs of biomass (‘fertility islands’).

Moreover, the desertification transition becomes (much) less abrupt in the presence of termite mounds, with a “jump” or gap between phases that is more than one order of magnitude smaller than in the absence of termite mounds (see Fig. S4). Thus, the differences between the two states in the bistability region are greatly reduced, and therefore so are the disruptive effects of the transition. Lastly, termite mounds shift not only the position of the thresholds, but also the location of the different patterns in the phase diagram (Fig. S3). Thus, mounds modify non-trivially the landscape, reinforcing the idea of termites as ecosystem engineers.

1.4 Sensitivity analysis: nutrients vs water

As explained above and in the main text, termites affect both water dynamics (reflected here in the infiltration effect via k_2) and nutrients (reflected here in the water-use efficiency, c). Here we explore to what extent each of these mechanisms, independently, is responsible for the observed behavior and patterns in our model. We therefore repeat the study of the system robustness when only one of the parameters is modified.

1.4.1 The role of the water-use efficiency, c

Improving c on mounds while leaving k_2 unchanged results in a steadily-changing phase diagram, in both directions, both quantitatively and qualitatively.

In both the decreasing- and the increasing-R directions, if the enhancement G_c is increased above a threshold (different for the increasing and decreasing directions), the curve shows the two discontinuities discussed in the previous section; Fig. S3). When the enhancement G_c is below the threshold however, the resulting curves show only one discontinuity, which is very close to the no-mound case (Fig. S5). This means that when the enhancement is below a threshold, vegetation on the mound shares the fate of off-mound vegetation. However, the final state of the ecosystem is fundamentally different from the no-mound case because vegetation in the whole ecosystem is generated on the mound and then is able to diffuse to the rest of the system. In this final pattern, unlike in the case when G_c is above threshold, vegetation on the mound is very similar to that off-mound (see Fig. S6 for low precipitation level and low improvements, G_c and G_{k2}).

As shown in Fig. S5, the threshold for the increasing- and decreasing-R directions differs. The different phenomenology observed for the same improvement factor in increasing- and decreasing-R directions is a consequence of the history-dependence enforced by the system's hysteresis.

1.4.2 The role of the infiltration effect, k_2

In the case of the infiltration effect, we find a similar threshold behavior as in the water-use efficiency analysis: there exist improvement thresholds (one in the increasing- and one in the decreasing-R direction) above which the phase diagram shows two discontinuities. However, the influence of G_{k2} seems to be weaker than that of G_c. For the increasing-R direction and G_{k2} below the threshold, the phase diagram is qualitatively similar to the no-mound case; only when G_{k2} is above such threshold is the second discontinuity generated (Fig. S5, bottom). However, that threshold is considerably higher than in the water-use efficiency enhancement case – for our parameter choices, improvements in k_2 of 67% (i.e. $G_{k2} = 3$) influence the diagram in a similar way as improvements of more than 10% in c (i.e. $G_c = 1.1$).

For the decreasing-R direction, there is a small but significant reduction in the location of the desertic discontinuity, and there are indications that when it happens it is the mound that drives the dynamics of the ecosystem (note the small density at the desertic transition in Fig. S5, top panel, indicative of an incipient second hysteresis loop). However, this effect is weaker than in the case of c, since very large enhancements are

needed to restore a wide, mound-only part of the phase diagram (e.g. $G_{k2} = 3$, i.e. 67% improvement, is still insufficient, see Fig. S5).

In summary, improvements in the infiltration effect alone are less likely to drive the dynamics of the ecosystem because large improvements are required in both directions.

1.4.3 Comparison with the complete case $G_c = G_{k2} = 1.5$

The cases in which one of the enhancements is kept as in Fig. S4 while the other is set to unity (i.e. no enhancement) are especially informative. They allow us to assess the performance of each parameter in comparison with the complete case (i.e. main case discussed in our paper), independently.

When we construct the phase diagram for the parametrization used for Fig. S4, now setting $G_{k2} = 1$ (that is, k_2 is not modified by the presence of termites), both the resulting increasing-R and decreasing-R diagrams show the two-discontinuity behavior. Moreover, the two directions are qualitatively identical and quantitatively very close to those in Fig. S4. Therefore, the realistic value chosen for the enhancement in the water-use efficiency (i.e. $G_c = 1.5$) is above the threshold and, by itself, is sufficient to produce the observed increase in the robustness of the ecosystem, as well as the homogeneous vegetation cover on mounds.

On the other hand, when now $G_{k2} = 1.5$ and $G_c = 1$ (that is, c is not modified by the presence of termites), the resulting phase diagrams are both qualitatively and quantitatively very similar to the no-mound case, with just a slight increase in vegetation density for the same R, and decrease in the location of the (apparently single) transition point. Therefore, the chosen enhancement in infiltration effect is under the threshold, and is not enough for the mound to affect significantly the behavior of the ecosystem. Moreover, even when the modification in k_2 reaches 67% of the off-mound value, the only-on-mound-vegetation part of the phase diagram is extended only a short range of R values, and the densities generated are very small (Fig. S5, bottom panel); therefore, the transition to desert is not substantially prevented or modified even by such a high value.

Thus, enhancement of the infiltration effect by itself, while helpful, is not enough (for realistic values) to generate a significant variation in the ecosystem's response to rainfall changes, nor the emergent patterns reported in the main text (i.e. mostly homogeneous vegetation on the mound).

1.5 Variable rain

Since, in most environments, rainfall is not constant throughout the year, we implemented a stochastic (dynamic) rainfall function $R = R(t)$ using actual data collected at MRC. These data show a dry season in which R decreases with time to a minimum

level R_{min}, and a wet season in which R varies showing three different local maxima (i.e. three humps) at the three most rainy months of the year (see Fig. S7).

The behavior described above can be modeled by means of a piecewise definition. For the specific MRC data, if $f(t) = R_0(\sin(2\pi t/6 - 3) + 1) + R_{min}$, then:

$$R(t) = \begin{cases} f(t) & \text{for} \quad t \leq 6.01 \\ 0.7\, f(t + \pi) & \text{for} \quad 6.01 < t \leq 8.66 \\ 0.9\, f(t) & \text{for} \quad t > 8.66, \end{cases} \tag{9}$$

where t is expressed in months and normalized so that $t \in [0, 12]$ (see Fig. S7 for the piecewise plot and Fig. 2 in the main text for the added stochasticity). To replicate MRC rainfall levels we would need $R_0 = 50$mm and $R_{min} = 10$mm (or 50/30 mm day^{-1} and 10/30 mm day^{-1}, respectively).

Note that our model uses generic values for the rest of the parameters (see Table S1). With this non-specific parametrization, the transition between dry and wet conditions occurs for $R \in (0.5, 0.7)$ (no-mound case). Therefore, we need to adjust R_0 and R_{min} to ensure that the rain function R(t) really explores the two seasons – vegetation-growth-challenging and vegetation-growth favorable seasons – also with such parametrization. Thus, for our parametrization, we keep the data-deduced shape for R(t), but adjust the parameters above to $R_0 = 20/30$ mm d^{-1} and $R_{min} = 10/30$ mm d^{-1}, which allows the system to experience both dry and wet conditions during a year. The variable rain produces patterns that are similar (albeit more noisy) to the ones obtained above (Fig. 2C-E in the main text). For temporal dynamics of the patterns showing the effect of seasonality, see Movies S1 and S2.

2 Empirical component

2.1 Study site

Field data were collected at the Mpala Research Centre (MRC) in the Laikipia highlands of central Kenya (36°52’ E, 0°17’ N, 1800 m elevation), where the ecological effects of

termite mounds have been well studied. Mean annual precipitation at this site from 1999-2013 was 657 mm ± 50 SEM. Rain falls in a trimodal annual pattern, with a major peak in April-May, minor peaks in July-August and November, and a short dry season from January-March (Fig. S7).

Our study site is underlain by level, topographically homogeneous, poorly drained "black-cotton" vertisol soils with high clay content (>50%), which comprise ~40% of the Laikipia ecosystem and many sites elsewhere in East Africa (including Nairobi National Park and parts of the Serengeti-Mara ecosystem) (37, 38). These soils support a characteristic flora with relatively few species. At our site, a single tree species (*Acacia drepanolobium*) accounts for >95% of canopy cover, and five species of perennial bunchgrasses constitute ~90% of understory cover (*Pennisetum mezianum*, *P. stramineum*, *Lintonia nutans*, *Themeda triandra*, and *Brachiaria lachnantha*) (38).

Another characteristic feature of black-cotton soils in this region is the presence of lenticular nests (mounds) created by *Odontotermes* spp. termites (subfamily Macrotermitinae, fungus-cultivating termites). These mounds were described as follows by Darlington (39) for the Embakasi Plain near Nairobi (see also (40,41)):

> "The pattern consists of regularly dispersed circular or oval patches of grass and herbs that have a different color from their surroundings. The patches are mostly 10-30 m in diameter with a surface slightly higher than the surrounding land (but usually by less than 50 cm). There is some difference in the plant species, but the color difference seems mainly to reflect the condition of the plants on the mounds, which remain green for longer into the dry season and become green more quickly when the rains begin."

At our site, the vast majority of mounds are 10-20 m in diameter and are conspicuously overdispersed, with an average distance between mounds of approximately 50-60 m ((21, 42); see Fig. 1A in the main text). The mounds themselves are treeless and grass-dominated, but trees occur at mound edges and throughout the inter-mound matrix (43). Mound soils are enriched in plant-available N and P relative to the surrounding matrix soils (42-44) and are permeated by networks of termite-constructed air shafts, passages, and tunnels (up to 15-cm diameter and 2-m below soil surface: (45)), which act as macropores that enhance water infiltration and aeration (reviewed in (19, 28)). These termite-induced properties generate pronounced spatial mosaics in plant growth and productivity across multiple trophic levels. As indicated in the quote above, understory plants are more productive on- vs. off-mounds at our site, as are *Acacia* trees growing at or near mound edges, and these local concentrations of resource availability propagate through the savanna food web to shape the distribution and activity levels of insects, spiders, lizards, and large herbivores (21,43,44).

2.2 Generality of termite-mound patterns & properties: is our field system representative?

The Macrotermitinae (including, prominently, Macrotermes and Odontotermes spp.) occur throughout sub-Saharan Africa and southern Asia (46), and their nest architectures and associated impacts on soils and vegetation are variable within and among genera (and even within species, depending on colony growth stage and/or environmental context) (47). As such, it would be impossible to develop a model that applied equally well to all types of termite mounds. However, our model is based on a limited number of fundamental mound properties that are exhibited not only by the Odontotermes mounds at our central Kenyan field site, but also among termite species spanning a wide range of taxonomic and geographic affiliations. The accumulated literature suggests that although these focal properties are not universal, they are sufficiently common to be considered a "syndrome," and thus that our model and conclusions are generally relevant in Old World tropical drylands (and not exclusively so, as various organisms in addition to termites engineer soils in similar ways (48)).

Specifically, we made three principal assumptions about termite mounds. The first, that mounds occur in overdispersed hexagonal lattices (21), has no qualitative effect on our model results (see main text) but is significant in the context of predicting catastrophic shifts; this is because from high altitude and at certain levels of precipitation (region 2 in Fig. 4B), the highly vegetated mounds dominate the images, producing spotted vegetation patterns similar to those thought to indicate imminent desertification in scale-dependent feedback models (12) (see our Fig. 1B,D; see also Fig. 2c in (3)). Although the phenomenon has never been systematically reviewed, regular overdispersion of termite mounds has been repeatedly documented dating back at least to the mid-20th century, when Macfadyen (49) described "termitaria peppering" in Somalia. Overdispersion of Macrotermes and Odontotermes nests have been reported from throughout sub-Saharan Africa (22,24,25,40,50-53). Similar overdispersed patterns are created by diverse termite taxa from Australia (54) to South America (55,56), and also by ground-nesting ant species from English meadows (57), Mediterranean shrublands (58), Neotropical rainforests (59), and North American deserts (60) and prairies (18,61). These patterns are generally attributed to resource competition among neighboring colonies, leading to hexagonal arrangements (24,57,58,60,62). Intriguingly, similar overdispersion has been shown for various landscape features whose origin is currently debated, including Namibian "fairy circles" (33,34), South American murundus (63,64), and South African heuweltjies (35,65,66). All of these structures have been attributed to social insects by some authors, and to alternative processes (including scale-dependent feedback) by others. Clearly, overdispersion of termite mounds and similar features is an extremely widespread occurrence rather than a peculiarity of any particular locality, ecosystem type, or soil-nesting organism.

Secondly, we assumed that termites enhance availability of moisture to plants. Many studies from diverse systems have shown that termites and other soil macrofauna can enhance soil porosity, infiltration, and soil-water storage (67-69; reviewed in (19,20,28,29)). An experimental study of Odontotermes in Sahelian drylands found that

”cumulative infiltration amounts, final infiltration rates, soil water content and porosity were larger and bulk density was smaller on termite plots as compared to non-termite plots” (29). As noted above, mound soils contain many macropores (in the form of vents and passages), the importance of which for infiltration has long been recognized (71).

Finally, we assumed that termite-mound soils were enriched in mineral nutrients relative to surrounding matrix soils, which in our model is the mechanism increasing the efficiency with which plants convert water into biomass. Nitrogen and phosphorus enrichment is a feature of Odontotermes mounds at our Kenyan field site, leading to enhanced foliar nutrient concentrations and productivity of plant and animal communities (21,42-44). Enrichment of both macro- and micronutrients appears to be a general property of large Macrotermitinae nests, which are often described as “nutrient hotspots” or “islands of fertility” that support exceptionally productive plant assemblages (19,20,27,71-74). Although it is likely that termites increase net nutrient availability of entire systems (as opposed to simply redistributing them), this is a difficult proposition to test due to the complex feedbacks involved (e.g., termites can influence soil formation, atmospheric nitrogen fixation by trees, etc.). Our main analysis assumed zero-sum dynamics, as this is conservative in terms of yielding a positive effect of termites on ecosystem robustness, and we show above that similar results are obtained if effects are not zero-sum.

2.3 Short-term versus long-term dynamics

We focused on the role of termite mounds in mediating the effect of rainfall on vegetation, but the vegetation will also reciprocally influence termite mounds. Long-term shifts in the climatic baseline will influence the occurrence and distribution of termite mounds: as vegetation biomass decreases, mounds may shrink, the distances between them may increase, and in the sustained absence of vegetation, mounds will eventually disappear from the system entirely. In this case, the “mound effects” of soil heterogeneity that we describe will be lost, and the incipient phases of vegetation recovery and patterning will likely be governed by SDF alone, as described in prior work (10, 12). However, this feedback has a different time constant (decades) than does the effect of shorter-term precipitation variability on vegetation (multiple months, seasons, or years). It is this latter phenomenon that we sought to capture, because it is relevant to the problem of increasing frequency/intensity of droughts predicted under many climate-change scenarios.

The limited available information about long-term dynamics of termite mounds suggests that mound legacies are likely to persist for (at least) years in the absence of active termite colonies, and hence that our model accurately describes (at least) the short-term properties of this system. When termite colonies die (as might occur during a particularly severe or long-lasting drought), the mound structures themselves remain and are often recolonized, with abandoned mound structures being the most likely sites for new colony establishment (75). As a result, individual termite mounds can be centuries old—sometimes older than the environments in which they are embedded, implying considerable robustness to environmental change. For example, large mounds in a

Nigerian rainforest were found to be older than the 200-year-old forest (76), while one in Zimbabwe was found to be ~700 years old (77). In our field system in central Kenya, we observe that "inactive" mounds are very similar to "active" mounds in terms of soil and vegetation properties, although we do not know how long this similarity lasts. Mound legacies are likely to persist even as mounds decay: erosion and leaching of enriched mound soils could locally maintain high productivity for long periods after termites are extinguished from the system (78).

The dearth of information in the literature about the dynamics of these processes, their durations, and their sensitivities to environmental conditions makes it difficult to rigorously model the longer-term dynamics. Future empirical and theoretical work along these lines would be useful, and important parallels could be drawn to other biological systems in which organizing regions emerge from scale-dependent activation-inhibition processes (e.g., head-formation in hydra (79)).

2.4 Data collection

Grass biomass. To evaluate our model prediction of greater vegetation biomass on versus off mounds, we quantified aboveground herbaceous biomass both on and off mounds using a standard disc pasture meter (81). On each of 35 mounds (N = 8-15 in each of three 4-ha plots, excluding mounds < 3-m diameter), we took six non-overlapping disc-pasture measurements; we then walked 15 m from the mound edge following a randomly chosen compass heading and again took six non-overlapping measurements. We averaged the six measurements from each on- and off-mound location and converted these means to biomass estimates following (81). We analyzed mean biomass estimates on- vs. off-mounds using a paired t-test in JMP 10.0 (SAS Institute, Cary, NC, USA).

Low-altitude aerial photography. To analyze fine-grain patterning of understory vegetation cover, we photographed three 30×30 m plots in January 2014. These plots were approximately evenly spaced across a ~2-km transect spanning a range of soil properties and tree cover representative of black-cotton-soil savanna at MRC; all plots were burned nine months prior to imaging, which reduced the grass canopy height and consumed litter that would otherwise have obscured vegetation patterning. Images were recorded using a high-resolution digital camera (Canon PowerShot S110) mounted on an 11-m carbon-fiber pole (Ron Thompson Gangster Carp Pole). The camera was mounted to the pole such that it could be held parallel to the ground at 10-m height. Images were recorded every second. Exposure was controlled manually to maintain consistency in changing light conditions. Within each plot, the camera rig was walked by the same individual (TCC) along parallel transects spaced 5-m apart (n = 7 transects/plot); this yielded a contiguous set of "large" images spanning approximately 3.4×5.9m, which collectively covered the entirety of each 30×30 m plot.

From this set of images, we selected 14 non-overlapping square subsections (1452 × 1452 pixels, using at most 2 subsections from each large image); these subsections spanned the ~2-km transect and were selected to comprise only grass and soil (i.e., no trees or termite mounds) and an absence of visible disturbance. We transformed RGB (red green blue) images to HSV (hue saturation value) and digitized the images into binary representations of the vegetation vs. soil based on the hue channel. We used the two-dimensional (2D) Fourier transform and a subsequent computation of the 2D periodogram (i.e., power spectrum; (82)), to provide a quantitative characterization of the spatial patterns (83). The amplitude values of the periodogram are a measure of the explicit spatial frequencies in the image. We then calculated the radial spectrum r (sum of the periodogram values on concentric ring-shaped regions of the 2D surface), to quantify the portion of image variances that can be accounted for by a simple cosine wave repeating itself r times (wavenumber) along a travel direction of the periodogram.

We compared the normalized radial spectra of binary images from the field site (n = 14) against the patterns produced by our model. From model simulations with stochastic seasonal rainfall, we selected snapshots of the vegetation in the dry season in different years (we used snapshots from January, corresponding to when the field images were collected in 2014). From these snapshots, we selected 16 subsections (200 × 200 pixels) in off-mounds areas (n = 192, 12 years × 16 subsections/year). We transformed the patterns of biomass density from the model into binary images (vegetation/bare soil, e.g. see Fig. 3C) according to a lower threshold found in the phase-plane analysis. We normalized the radial spectra for: (a) the wavenumber, by dividing r by the size of the domain in the analyzed image (ca. 1.5 m for field images and 2 m for simulations); and (b) the amplitude of the radial spectrum, by dividing by the maximum of the mean.

2.5 Results

Overall mean grass biomass was 4008 kg/ha off mounds and 5304 kg/ha on mounds ($t = 5.32$, $df = 34$, $P < 0.0001$). When we calculated percent differences for each paired on- and off-mound location, grass biomass was 42.2% greater, on average, on mounds than in corresponding off-mound locations. This agrees with our model prediction of enhanced vegetation biomass on mounds.

We found that the spatial frequencies of the model-simulated vegetation patterns agreed with the characteristic spatial frequencies in the observed vegetation pattern at our field site, as shown by a peak of the radial spectrum at six cycles m^{-1} (Fig. 3E main text). Furthermore, the shape of the radial spectrum (specifically the peak of the mean standardized r-spectrum at a low wavenumber and the fat tail) is characteristic of a spotted pattern (84).

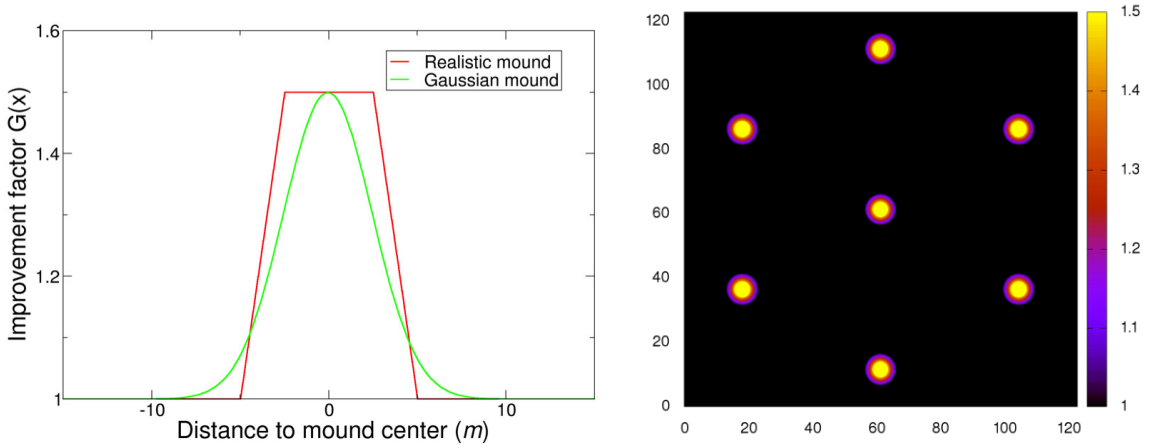

Fig. S1.

Left: To implement the improvement in water-use efficiency and infiltration, we explore both a flat-type improvement (red curve) and a gaussian improvement (green curve). They yield qualitatively similar results but the flat improvement is a more realistic description of the system. Right: Spatial distribution of the improvement factor G_c in the hexagonal mound configuration, for a system 120 × 120m wide. Both panels are parametrized such that the maximum improvement factor is 1.5.

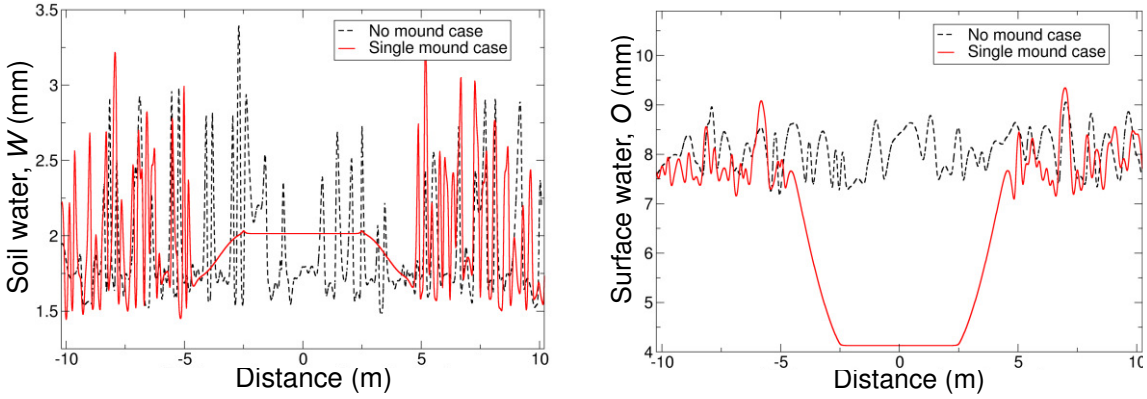

Fig. S2. Model output transects for the soil water, W (left), and surface water, O (right), densities, measured relative to the center of the mound in a 20.48m wide system. As in the case of the plant density profile, P (see main text), the mound alters not only the surface it covers, but also its most immediate environment. In this case, the radius of influence of the mound is close to 6m, i.e. one meter longer than the mound radius. As expected, O decreases as the center of the mound is approached (right panel); on the other hand, the effect of the mound on W depends on the implementation of R; indeed, if R changes with time (see section 1.5), on-mound W varies from being larger to smaller than off-mound values (the latter due to the higher growth and therefore water demand by the mound). As in the P panel of the main text (Fig. 2B), in these simulations $dx = 2 \times 10^{-2}$m, $D_P = D_W = 10^{-5}$m^2/*d*, and $D_O = 10^{-3}$m^2/*d*.

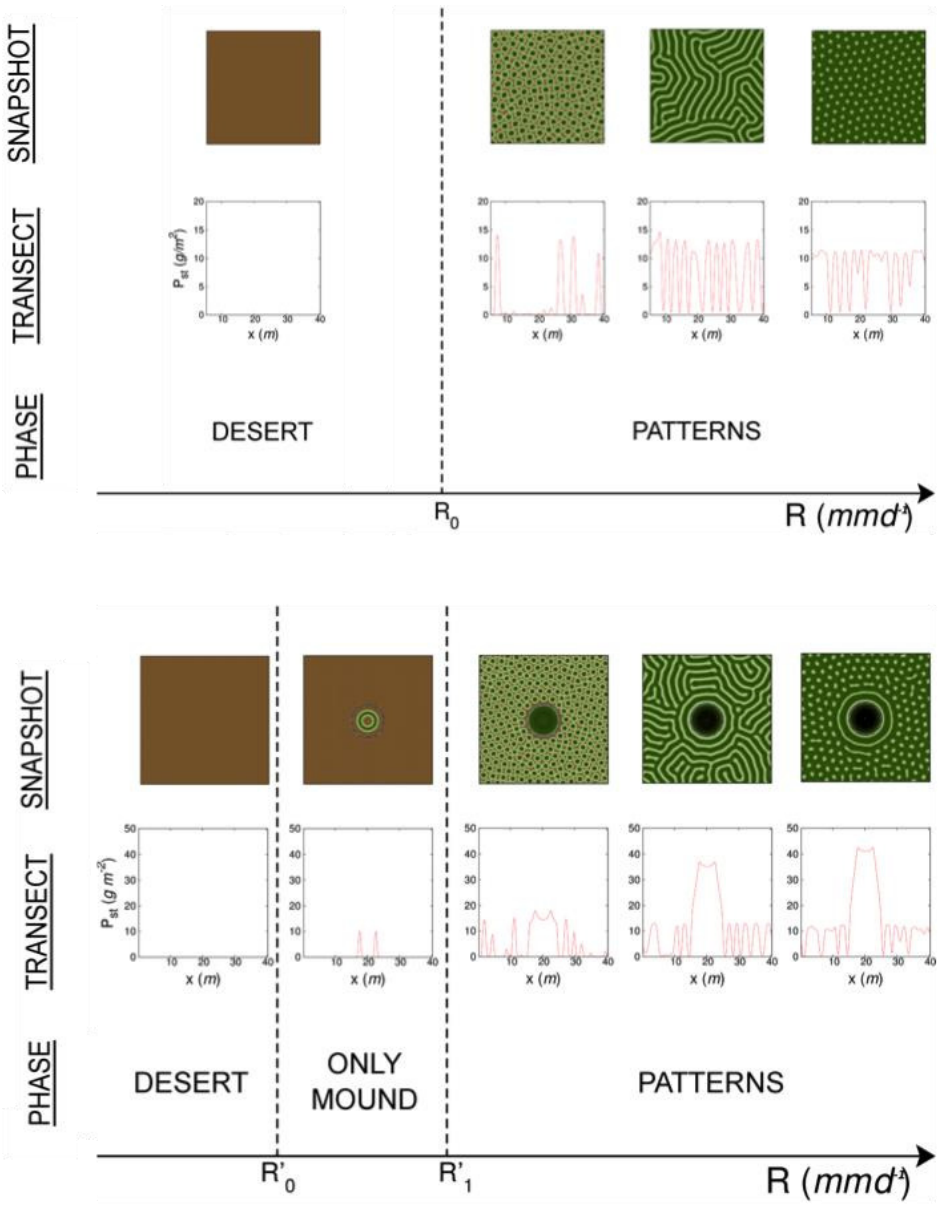

Fig. S3.

Plant spatial distributions for the original model (top) and for our modified model with one termite mound (bottom, for which model 1 has been used together with the parameterization in Table A.1 and Fig. S5). Top: For low R, the system collapses to a desert state; as R is increased beyond a threshold, R_0, patterned vegetation emerges throughout the system, with the emergent pattern depending on R; finally, for high precipitation, the system is homogeneously covered by vegetation. Bottom: In the presence of termites, overcoming a first threshold, R_0', allows vegetation to survive on the mound; this vegetation covers initially a reduced part of the mound surface, and as R increases not only does the covered radius increase, but once a second threshold, R_1', is crossed, vegetation is regenerated in the rest of the ecosystem. Patterns off the mound are similar to those obtained with the original system. For any R, biomass (P_{st}) is larger on the mound than off the mound. For both panels, the transect and snapshot data have been extracted from Fig.S5.

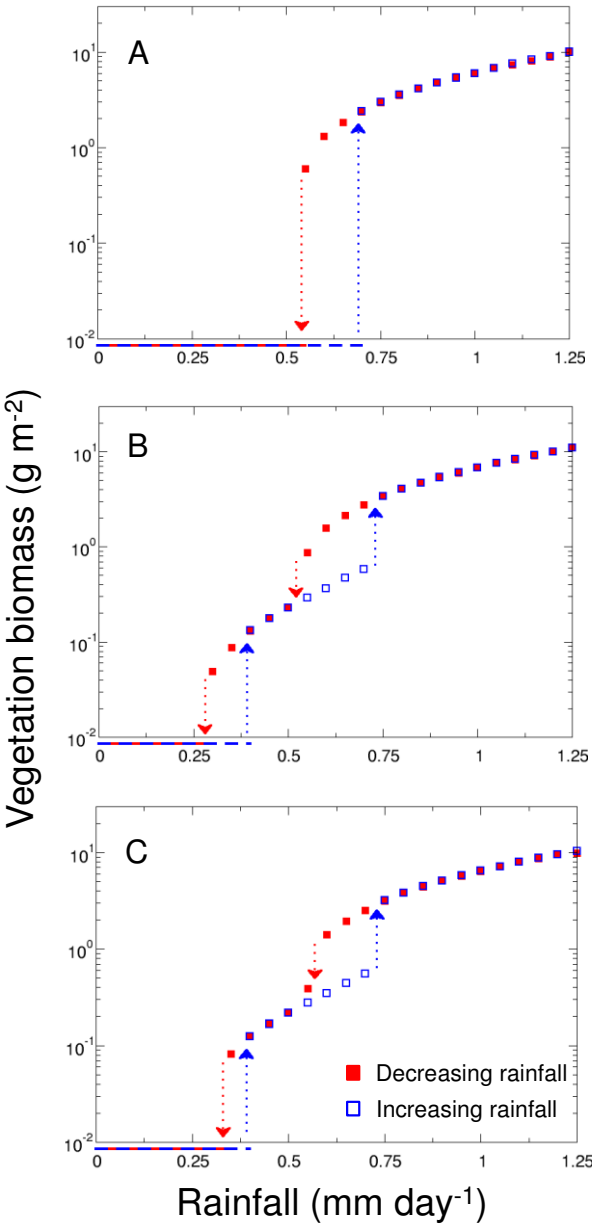

Fig. S4.

(A) For the original, mound-free system, the desertification threshold is located at $R_{0,inc}$ = 0.70(5) as R increases, and at $R_{0,dec}$ = 0.55(5) as R decreases; in between, there is a bistability region. (B) For Model 1 (termites have only positive effects), the desertification threshold shifts to $R_{0,inc}'$ = 0.40(5) and $R_{0,dec}'$ = 0.30(5); this threshold gives way to a state where only the mound is vegetated; once a second threshold is crossed ($R_{1,inc}'$ = 0.75(5) and $R_{1,dec}'$ = 0.55(5)), vegetation grows in the rest of the system. (C) For Model 2 (the effect of termites is 'zero-sum') $R_{0,inc}''$ = 0.40(5) and $R_{0,dec}''$ = 0.35(5), and $R_{1,inc}''$ = 0.75(5) and $R_{1,dec}''$ = 0.60(5). Note that in this semi-logarithmic plot the blue and red line marks the zero-density case. For the three panels, dx = 2×10^{-1}m, $D_P = D_W = 10^{-3}$, $D_O = 10^{-1}$ ($m^2 d^{-1}$); $G_c = G_{k2}$ = 1.5; all other parameters are as in Table A.1. The error bars provided for the location of the discontinuities (numbers in parentheses) reflect variability across replicates due to the bistability present in the hysteresis area.

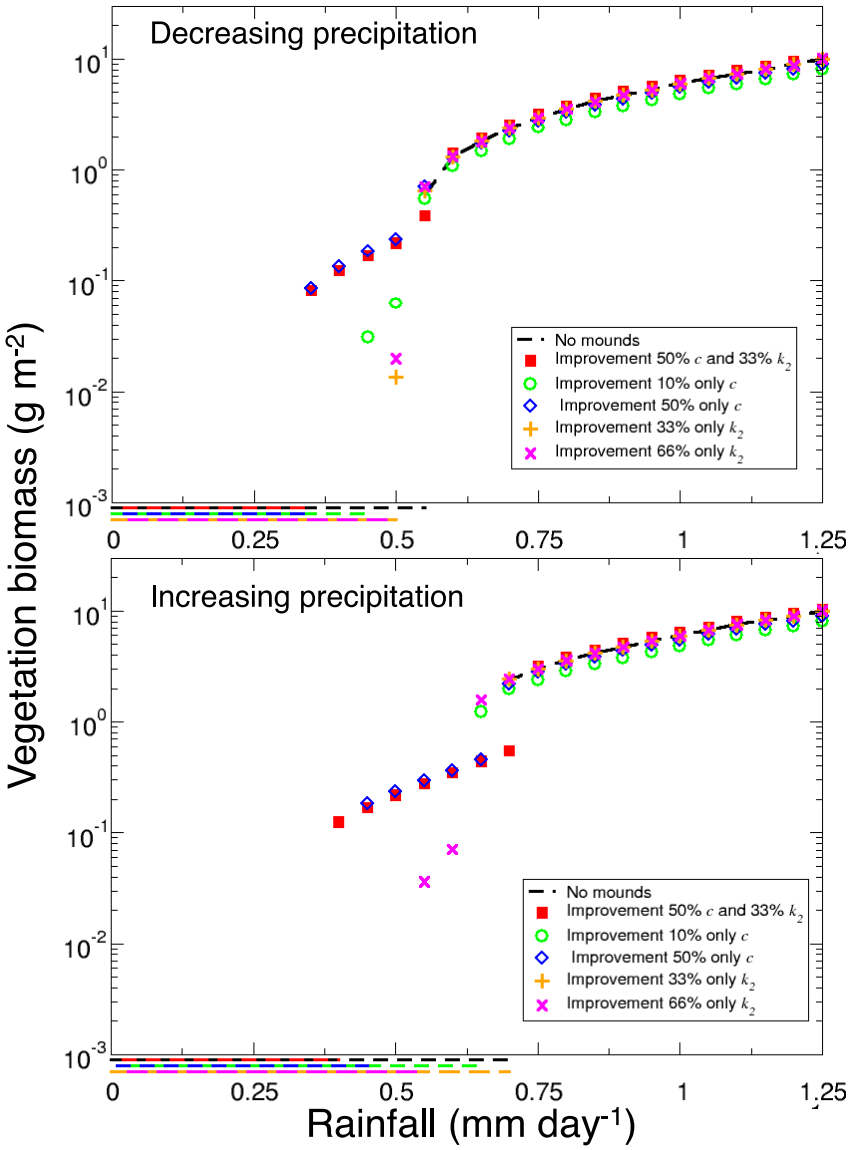

Fig. S5.

Decreasing-R (top) and increasing-R (bottom) branches of the phase diagrams obtained without mounds (black line), and with mounds with different improvement factors in: both c and k_2 (red squares), only c (blue diamonds and green circles), or only k_2 (orange and pink crosses). As in previous plots, the semi-logarithmic representation requires for the extinct-vegetation points to be represented with lines out of the diagram. Both panels used the parametrization for space mesh and diffusivities described in Fig. S5.

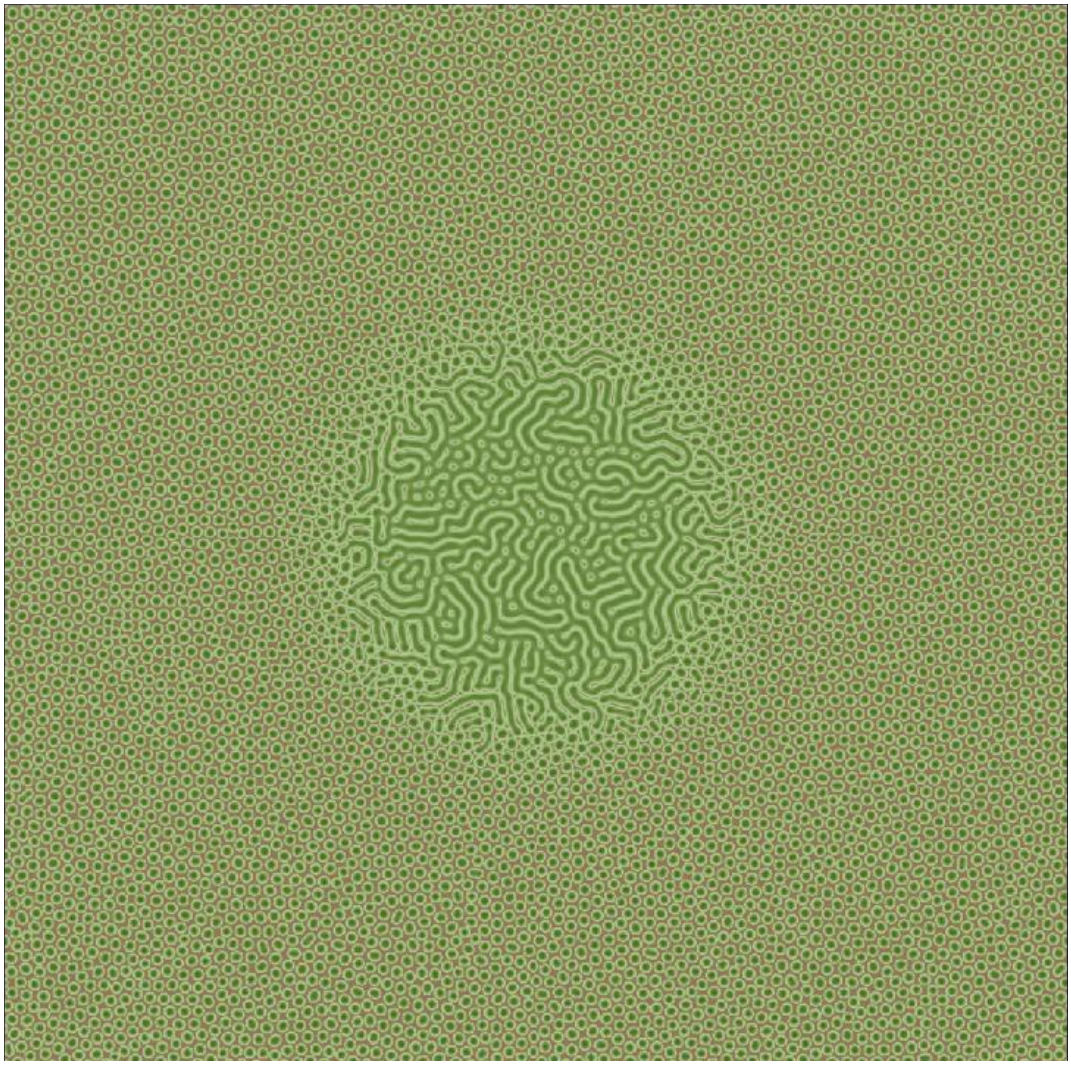

Fig. S6.

Depending on the level of precipitation and on the improvement parameters, a mound can be covered by vegetation ranging from overdispersed spots to labyrinths, to overdispersed gaps and to homogeneous cover; for certain levels of improvement and low precipitation levels, concentric rings can arise. Here, for precipitation R = 0.8 which produces spot-like vegetation off the mounds, and for improvement parameters $G_c = G_{k2} = 1.2$, the mound is covered by labyrinthine vegetation. All other parameters are as in Table S1.

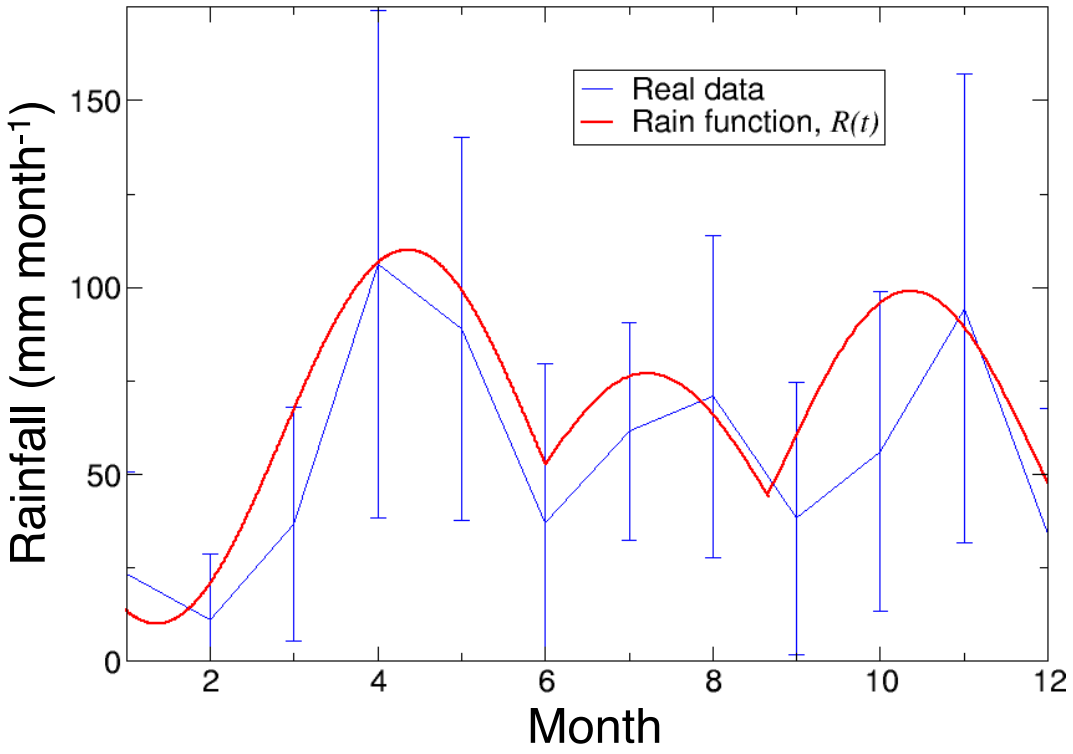

Fig. S7.

Real data (blue) and functional approximation (red) for the rainfall levels measured in MRC. The red curve corresponds to R(t), Eq. (9), with R_0 = 50mm and R_{min} = 10mm. For our simulations, we switched those two parameters to precipitation rates and decreased their value in order to bring the range of R(t) to the standards set by our chosen parametrization.

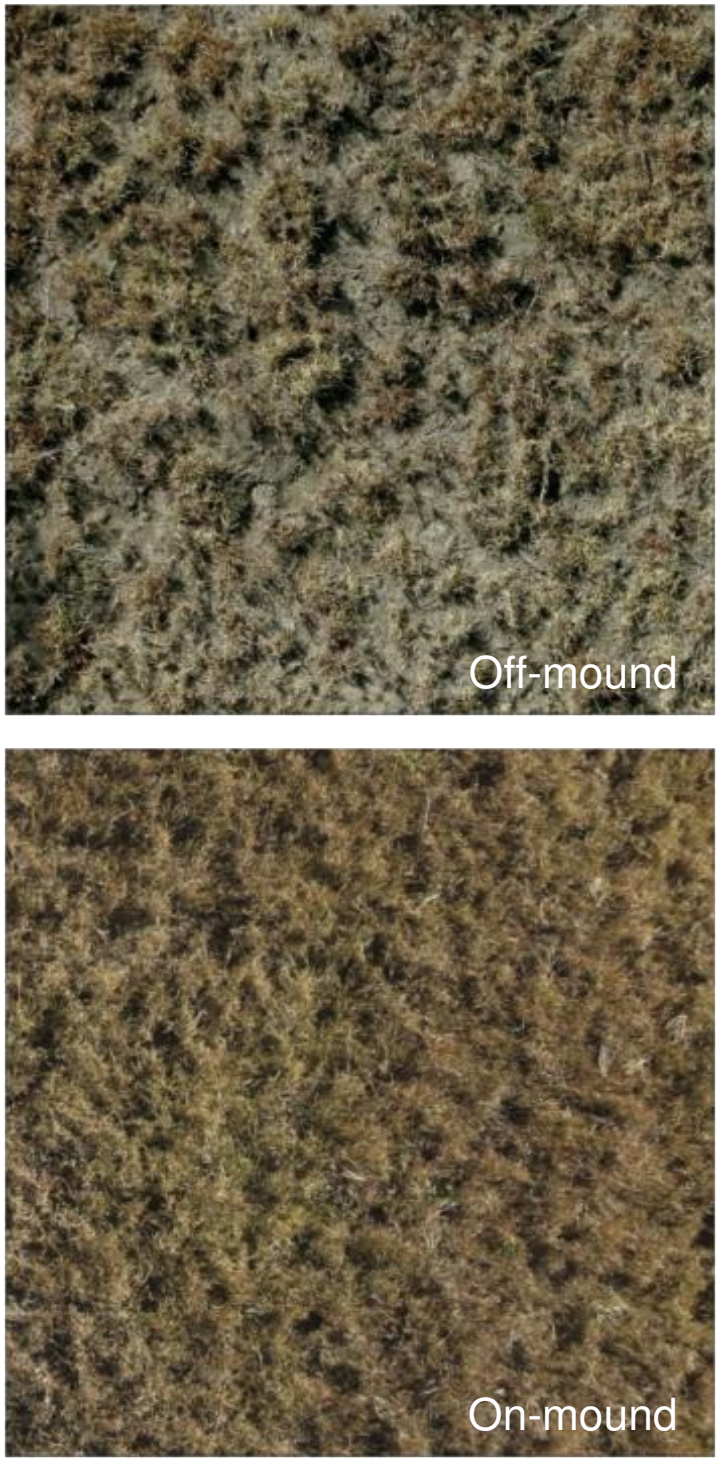

Fig. S8.

Off-mound vegetation (top) is patchy; on-mound vegetation (bottom) is homogeneous. Pictures shown are of 2m×2m regions.

Table S1.

Table of notations, parameters and values. The values are those from (7) except for the diffusion rates, which have been tuned to obtain pattern wavelengths comparable to those from the data, and the perturbation strength. The diffusion rates used in (7) are shown in black; the various values used in this paper are shown in blue. The improvement parameters introduced in the modified model are also shown in blue.

Parameter	Meaning	Value (Units)
c	Uptake-growth conversion factor ('water-use efficiency')	10 (g mm^{-1} m^{-2})
g_{max}	Plant maximum uptake rate	0.05 (mm g^{-1} m^{-2} d^{-1})
k_1	Water uptake half-saturation constant	5 (mm)
d	Mortality rate	0.25(d^{-1})
α	Maximum infiltration rate	0.2 (d^{-1})
k_2	Saturation constant of water infiltration ('infiltration effect')	5 (g m^{-2})
W_0	Part of soil infiltration capacity for P = 0	0.2 (—)
r_W	Evaporation rate	0.2 (d^{-1})
D_P	Plant diffusivity/dispersal constant	10^{-1}; 10^{-3}; 9×10^{-5}; 10^{-5}; 2.5×10^{-6}(m^2 d^{-1})
D_W	Underground water diffusivity constant	10^{-1}; 10^{-3}; 9×10^{-5}; 10^{-5}; 2.5×10^{-6}(m^2 d^{-1})
D_O	Surface water diffusivity constant	10^{2}; 10^{-1}; 9×10^{-3}; 10^{-3}; 2.5×10^{-4}(m^2 d^{-1})
R	Precipitation rate	Control parameter (mm d^{-1})
G_c	On-mound water-use efficiency improvement	Varies between 0% and 50%
G_{k2}	On-mound infiltration effect improvement	Varies between 0% and 67%
ΔP	Perturbation strength, added to random location's P	5 (g m^{-2})

Movie S1

Sequence of snapshots obtained with the modified model with one mound, stochastic rainfall rate, and parameterization as in Fig. 2. The red solid circle in the rainfall function panel represents the actual value of R(t), whereas the mean value is given by the brown curve. This movies shows the whole mound and surroundings (~20m lateral size). Note that, with this dynamic rainfall function, there is a realistic delay between the rainfall rate and the effects on the vegetation; thus, only well into the dry season the system loses most of its vegetation, which resists on the mound and as underground biomass. Once the rain season is well underway, vegetation is regenerated in the whole ecosystem, with patterns that change as water availability changes.

Movie S2

Sequence of snapshots obtained with the modified model with one mound, stochastic rainfall rate, and parameterization as in Fig. 2. The zoom is at 2m×2m, as in Fig. 2E. The red solid circle in the rainfall function panel represents the actual value of R(t), whereas the mean value is given by the brown curve. This movie shows a zoom of the area close to the mound boundaries.